heritage

MDPI

Article

Contribution to the Understanding of the Colour Change in Bluish-Grey Limestones

Teresa P. Silva [1,*], Daniel de Oliveira [1,2], João P. Veiga [3], Vitor Lisboa [1], Jorge Carvalho [1], M. Alexandra Barreiros [4], Mathilda L. Coutinho [5,6], Eduardo Salas-Colera [7,8,9] and Rogério Vigário [10]

1 LNEG (National Laboratory for Energy and Geology), Mineral Resources and Geophysics Research Unit, Estrada da Portela, Apartado 7586, 2610-999 Amadora, Portugal; daniel.oliveira@lneg.pt (D.d.O.); vitor.lisboa@lneg.pt (V.L.); jorge.carvalho@lneg.pt (J.C.)
2 Mineral Resources Expert Group, EuroGeoSurveys, Rue Joseph II 36-38, P.O. Box 7, 1000 Brussels, Belgium
3 Department of Conservation and Restoration, CENIMAT/i3N, Materials Research Centre, NOVA School of Science and Technology, FCT NOVA, 2829-516 Caparica, Portugal; jpv@fct.unl.pt
4 LNEG (National Laboratory for Energy and Geology), Materials for Energy Unit, Estrada do Paço do Lumiar 22, 1649-038 Lisboa, Portugal; alexandra.barreiros@lneg.pt
5 Laboratório Hercules—IFAA, Universidade de Évora, Largo Marquês de Marialva 8, 7000-809 Évora, Portugal; mathildal@gmail.com
6 VICARTE—Vidro e Cerâmica para as Artes, Faculdade de Ciências e Tecnologia, Universidade NOVA de Lisboa, Quinta da Torre, 2829-516 Caparica, Portugal
7 Spanish CRG BM25 SpLine Beamline, The European Synchrotron (ESRF), 71 Av. des Martyrs, 38000 Grenoble, France; eduardo.salas.colera@gmail.com
8 Instituto de Ciencia de Materiales de Madrid (ICMM-CSIC), Sor Juana Inés de la Cruz 3, 28049 Cantoblanco, Madrid, Spain
9 Physics Department, Universidad Carlos III de Madrid (UC3M), Av. de la Universidad 30, 28911 Leganés, Madrid, Spain
10 MVC-Mármores de Alcobaça, Ataíja de Cima, 2460-713 Alcobaça, Portugal; rogerio@mvc.pt
* Correspondence: teresa.pena@lneg.pt

Citation: Silva, T.P.; de Oliveira, D.; Veiga, J.P.; Lisboa, V.; Carvalho, J.; Barreiros, M.A.; Coutinho, M.L.; Salas-Colera, E.; Vigário, R. Contribution to the Understanding of the Colour Change in Bluish-Grey Limestones. *Heritage* **2022**, *5*, 1479–1503. https://doi.org/10.3390/heritage5030078

Academic Editors: Ákos Török and Miguel Gomez-Heras

Received: 19 April 2022
Accepted: 28 June 2022
Published: 30 June 2022

Abstract: Bluish-grey limestones have been extensively used as ornamental stones for decoration purposes in buildings, as well as in works of art, and accordingly, have been the target of intense exploration. In Portugal, the Jurassic limestone massif known as the Maciço Calcário Estremenho (MCE), has been the source of grey-coloured ornamental stones, namely the *Azul Valverde* (one of the most well-known bluish-grey limestones) and *Atlantic Blue* varieties, both of which may undergo colour changes in outdoor environments. In this sense, it is important to understand the sudden colour change from bluish-grey to yellow/beige in the same limestone block in a quarry, or even, what happens to the colour when polished limestone is placed outdoors. This study was undertaken using various techniques, namely XRF (X-ray fluorescence spectrometry), XRD (X-ray diffraction), SEM (scanning electron microscopy), DTA–TG (differential thermal analysis/thermogravimetry) and colourimetry. Synchrotron radiation was also used at the European Synchrotron Radiation Facility (ESRF, Grenoble, France) where XANES (X-ray Absorption Near Edge Structure) spectra at Fe *K*-edge were collected to ascertain the speciation state of Fe in different coloured zones of the limestone, previously checked by EDXRF (energy dispersive X-ray fluorescence). The presence of Fe^{2+} and Fe^{3+} are responsible for the greyish and yellow/brown colour, respectively. On the other hand, the UV radiation from the sun causes a quickened and severe bleaching/fading on the dark blue/grey polished limestone.

Keywords: built heritage; ornamental stone; dark limestone; bleaching/fading; iron; XANES

1. Introduction

Carbonate rocks, in general, display light colours such as whitish, beige, or yellowish. However, they may also exhibit darker tonalities, namely greyish to black, bluish, or even

reddish, depending on the nature and content of impurities scattered throughout the rock mass. Rock colour can be considered a complex concept, as it depends on the perception of the observer, the source of illumination, the characteristics of the object, and the environment in which light radiation can be absorbed, filtered, reflected, refracted, or interfere with each other [1]. Despite this complexity and even subjectivity, the colour of natural stones is a major characterization factor due to its influence on the aesthetic and commercial value of the rock [2–4].

The consequence of trends in architecture for the use of dark colours in decoration of both interiors and exteriors (e.g., [5,6]), results in the growing demand for natural, grey-coloured stones with several finishings currently in use: polished, bush-hammered, flamed, and scratched, among others. However, the colour bleaching (fading), more visible in the dark colours, is a concern for both limestone producers and customers, passing through art conservator-restorers, because it is a requirement that the rock colour remains the same during the lifetime of the construction (e.g., [7]).

One example of such a grey-coloured ornamental stone comes from the Jurassic limestone massif in Portugal known as the *Maciço Calcário Estremenho* (MCE). The commercially designated *Azul Valverde* (Valverde Blue) variety, also known as *Azul Mónica* [8], is one of the most internationally recognised bluish-grey limestones from Portugal that has been used as a reference grey limestone in the ornamental stones market. Other bluish-grey facies of commercially marketed ornamental limestones are the *Atlantic Blue* and *Azul Moleanos* varieties. Of these, this study is focused on the *Azul Valverde* and *Atlantic Blue* types.

The constant exposure to natural weathering (solar radiation, temperature variation**,** water percolation, air pollution, biological agents) causes several types of damage including physical weathering, such as microcracking and disintegration, and chemical weathering, such as discoloration and dissolution of component mineral grains [9–13]. Limestone catastrophic deterioration results in black crusts, scaling, flaking, blistering, granular disintegration, and alveoli [14], making colour alteration one of the most evident signs of deterioration in heritage materials.

The colour of limestones and sedimentary rocks in general is usually controlled by accessory minerals, plus compounds of iron and organic carbon [15]. Concerning the bluish-grey limestone, the discolouration process could be the result of weathering (pyrite oxidation) with progressive formation of gypsum crystals on the surface and subsequent biocolonisation [16]. This is usually associated with epigenetic fluid percolation driven by fractures and by marl-carbon sedimentary lamina (e.g., [17]), or by the presence of clay minerals [18], but it remains unclear which factors lead to the occurrence of each colour [16]. Indeed, recent studies regarding the mechanisms of discolouration of a bluish limestone from the MCE were performed, assuming that the bluish colour origin is due to the presence of dispersed organic matter that was introduced in the rock prior to early carbonate cementation processes by the percolation of hydrocarbon-rich fluids [19]. This author characterised the rock as a quite homogeneous calcarenite, very compact and almost completely cemented by carbonate, with accumulation of insoluble residues together with pyrite (FeS_2) and darker compounds (oxides/hydroxides) not identifiable by microscopic observation. The laboratory simulation of chemical reactions under oxidising, acidic and oxidising plus acidic conditions, led to conclude that the oxidation of the organic compounds was the main cause of colour transformation (partial discolouration) in the limestone. On the other hand, the staining of white marble was attributed to the presence organic matter in the form of pyrite and hematite crystals, yet these were shown to have no significant influence on the discolouration [20]. Recently, a laser cleaning process of a deeply darkened limestone surface (black crust) collected from the historic entrance gate of Castello Svevo, Bari, Italy gave rise initially to a yellowish/brownish surface and, after a new treatment, a whitish one [21].

Furthermore, colour changes of the natural stone could be attributed to the exposure to UV light [7,22–24] causing fading; photonic effects (mainly UV radiation) may be

particularly harmful as observed, for example, in outdoor-exposed tiles/panels [25]. Additionally, grey carbonaceous limestones increase their value of lightness by oxidation and fading/bleaching by the sun [24]. The colour fading has a negative economic impact in the ornamental stone industry and in the field of built heritage. The fading of the blue marble in the Paço Ducal de Vila Viçosa is one of the most notorious cases. For decades the façade was thought to be made of a yellowish-white coloured stone. After a cleaning intervention, the extraordinary blue and white stonework was re-discovered (Figure 1). Other examples of historic structures made of limestone are for instance, the arch over the tunnel between the sacred area and the stadium in Olympia Greece, the Cheops Pyramid in Egypt, the Parliament building of Budapest, Hungary [13], the Convent of Christ in Tomar, Portugal [26], Worcester College, Oxford, UK [14], the Master Valentim's fountain, Rio de Janeiro, Brazil [10], or even limestone sculptures, namely St. John the Baptist, St. Paul and The Virgin and the Child from 16th century, and Musician Angel (15th century) [27].

Figure 1. Façade of the Paço Ducal de Vila Viçosa (Portugal): (**a**) before and (**b**) after the cleaning intervention (©Fundação da Casa de Bragança).

In the shown context, the aim of this study is to contribute to the understanding of the mechanisms responsible for the colour change, namely, the fading observed in two bluish-grey ornamental limestone varieties commercially designated as *Azul Valverde* and *Atlantic Blue* when these are exposed to normal weathering conditions. To address this major goal, focusing on polished tiles/slabs placed in outdoor environments and in the quarry blocks (variation between bluish-grey and yellow side by side in the same limestone block), a study was undertaken utilising various techniques including synchrotron radiation at the European Synchrotron Radiation Facility-ESRF, in Grenoble, France; in this novel approach, the methodology applied to limestones allowed us to disclose the iron speciation in those sought-after ornamental stones.

The main accomplishment of this paper is the relation, on the one hand, of the presence of Fe^{2+} and Fe^{3+} with the greyish and yellow/brown colour, respectively, and on the other hand, of the quickened and severe bleaching/fading of the dark blue/grey polished limestone with the UV radiation from the sun.

2. Geological Setting and Features of the Bluish-Grey Limestone

The MCE is a geomorphological unit corresponding to a Jurassic limestone massif that covers an area of 900 km² in the centre of Portugal, approximately 150 km to the north of Lisbon (Figure 2). The MCE falls within the paleogeographic context of the Lusitanian Basin, which developed in the non-volcanic rift margin of western Iberia under a generalised extensional tectonic regime associated with the opening of the North Atlantic Ocean. After the Upper Cretaceous, it becomes uplifted in relation to the surrounding regions due to the Alpine compressive tectonics whose major effects occurred during the late Miocene [28–31].

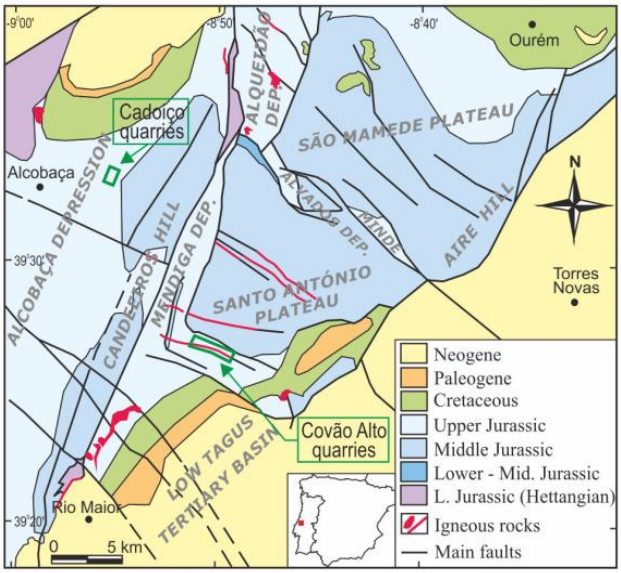

Figure 2. Geological map of the Maciço Calcário Estremenho, with the location of the Covão Alto ("*Azul Valverde*" stones) and Cadoiço ("*Atlantic Blue*" stones) quarrying areas (adapted from [32]).

Three major families of faults, oriented NNE–SSW, NW–SE, and NE–SW, highlight the close existing relationship between morphology and tectonics in the MCE. They were active during the extensional phases of the North Atlantic opening and were reactivated in reverse or strike-slip mode by the Alpine compression. In addition to these faults, the MCE is affected by low amplitude, smooth folding, and by a moderately intense fracture network that follows the three orientations mentioned above [32]. Rocks in the MCE are distributed, in terms of age, from the Lower Jurassic to the Cretaceous. However, most of its extension is occupied by carbonate rock formations of the Middle and Upper Jurassic whose lithostratigraphy is well established from the works of Manuppella and Azerêdo [33–35].

To meet ornamental stone market demands, limestones from the MCE have been the target of intense exploitation since the 1980s. The *Azul Valverde* is exploited at the "Covão Alto" quarrying area, near Alcanede (Santarém district) (Figure 2). It is also known as the "Malhada" or "Valverde" area, despite the fact that the Valverde village is situated some kilometres further north. The stone exploited here belong to Upper Jurassic series, namely the Montejunto Formation of Middle to Upper Oxfordian age ("Camadas de Montejunto") according to sheet 27-C of the Portuguese Geological Map at 1:50,000 scale [34]. This lithostratigraphic unit corresponds to a sequence of grey limestones and marls, more or less dark in colour, with thickness larger than 80 m. At the Covão Alto quarrying area, the exploited rocks are peloidal and intraclastic marly mudstones, wackestones and packstones with varying content of bioclasts and oolites, sometimes with nodular appearance.

The quarries are laid out parallel to a dolerite dike, which intruded a normal fault oriented WNW–ESE. It controls the attitude of bedding: dips around 40° S near the fault

and between 10° to 20° S when outside the associated drag fold. The first stones exploited here were the ones closer to the dike, where they were tougher and darker in colour.

Thickness of the beds ranges from some centimetres to 1 m, often with organic-rich marly laminae between them. As these laminae maintain the mechanical coherence among the strata, it is possible to produce blocks for ornamental purposes up to 2 m thick. Despite the bluish-grey colour denoted by the *Azul Valverde* ornamental variety, sudden colour changes to beige can be observed in the quarry walls affecting not only several layers, but also along a single layer (Figure 3).

The technical description of the *Azul Valverde* ornamental rock is a grey-blue limestone with small, lighter patches, with coarse elements, calciclastic and slightly bioclastic being constituted by 93% of calcite, 3% of dolomite and 4% of quartz [36]. Chemical analysis published by these authors showed contents of 1.78% SiO_2, 0.87% Al_2O_3, 0.60% Fe_2O_3, vestiges of MnO, 51.42% CaO, 1.31% MgO, 0.18% Na_2O, 0.16% K_2O, and 42.53% of LOI. When compared to other Portuguese limestones, *Azul Valverde* and *Azul Moleanos* have the highest iron content, 0.6% Fe_2O_3 [36]. The presence of iron, can provide a great diversity of colours to minerals and geomaterials, as known (e.g., [37,38]): goethite, α-FeO(OH), and siderite, $FeCO_3$, form yellow-brown ochre; hematite, α-Fe_2O_3, depicts a characteristic grey colour when well crystallised and a red tonality in soils (regoliths); vivianite, $Fe_3(PO_4)_2 \cdot 8H_2O$, displays either a blue or a purple colour [39]; and green tonalities are common for olivine, $(Mg,Fe)_2SiO_4$. Moreover, in what concerns sulphides, disseminated pyrite, FeS_2, gives a grey colour to a carbonate matrix [40].

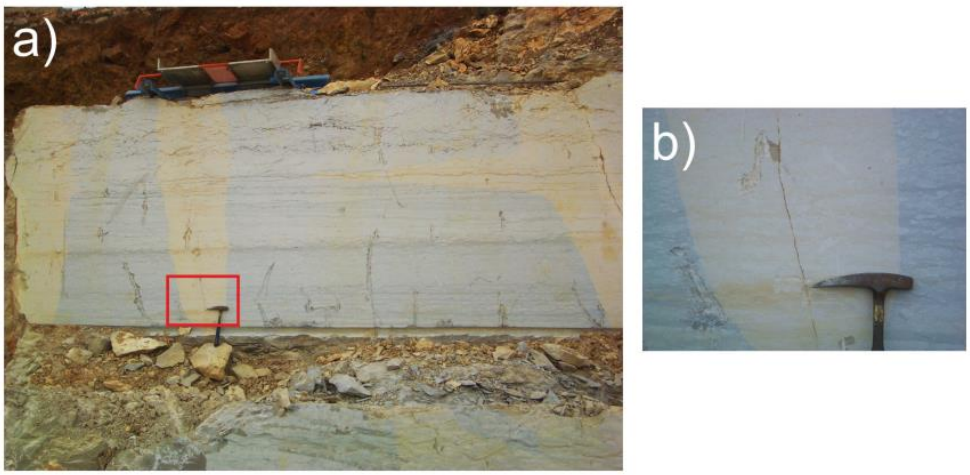

Figure 3. Sudden colour changes from greyish-blue to beige in a quarry of the Covão Alto area. In (**a**) vertical and horizontal colour changes across and parallel to layering; (**b**) detail of (**a**) where it is evident that the colour change corresponds to an alteration halo parallel to a thin vertical joint.

The *Atlantic Blue* ornamental variety, also known as *Azul Cadoiço* [41], is very similar to *Azul Valverde*. It comes from the Cadoiço quarrying area (Figure 2) located near Alcobaça (Leiria district), which also are exploiting the Montejunto formation. The limestones are very similar to the ones exploited in Covão Alto: marly wackestones, packstones, and grainstones with a bluish-grey colour. Thin clayey laminae are interbedded with decimetre to metric-thick, marly limestone beds oriented NNE–SSE and dipping 15°W.

Both limestones have low water absorption at atmospheric pressure, 0.5% [8] (p. 347) and 0.8% [42], respectively. *Atlantic Blue* presents a light grey colour, slightly bluish and brownish shadows [42].

3. Materials and Methods

Several samples of *Azul Valverde* and *Atlantic Blue* limestone were selected for the present study (Table 1). Some polished samples were exposed to natural weathering conditions (Figure 4, assigned with an * in Table 1) and analysed through various techniques,

before and after being exposed, to understand the type and severity of this degradation in the dark colour of the limestone. Other samples were analysed as collected in the quarry (unpolished) or after being polished. Polychromatic fragments were chosen, where the variation side by side between bluish-grey/brown/yellow or bluish-grey/yellow was well pronounced, to disclose the reason of that colour variation, induced by the fluids' percolation.

Table 1. Characteristics of the limestone fragments and analytical technique(s) used in their study; *Azul Valverde* (AV) and *Atlantic Blue* (AB); X-ray fluorescence spectrometry in wavelength dispersive mode (XRF-WDS); X-ray diffraction (XRD); scanning electron microscopy with energy dispersive spectroscopy (SEM/EDS); differential thermal analysis/thermogravimetry (DTA–TG); X-ray absorption near edge structure (XANES) and energy dispersive X-ray fluorescence (EDXRF); naturally weathered samples are assigned with *.

Quarry	Limestone Designation	Sample Characteristics	Reference	Analytical Technique
Covão Alto	*Azul Valverde*	Polished, greyish	AV 27 *	XRF-WDS; XRD; SEM/EDS; colourimetry
		Polished, greyish	AV 43 *	XRF-WDS; colourimetry
		Polished, polychromatic	AV Yellow area	SEM/EDS
			AV Bluish-grey area	SEM/EDS
		Unpolished, polychromatic	AV Yellow (1) area	XRD; XANES; EDXRF
			AV Brown (2) area	XRD; XANES; EDXRF
			AV Bluish-grey (3) area	XRD; XANES; EDXRF
		Unpolished	AV Bluish-grey (A)	XRD; DTA–TG; XANES
		Unpolished	AV Yellow (B)	XRD; DTA–TG; XANES
Cadoiço	*Atlantic Blue*	Polished, greyish	AB 9 *	XRF-WDS; XRD; SEM/EDS; colourimetry
		Polished, greyish	AB 48 *	XRF-WDS; colourimetry

Figure 4. *Azul Valverde* (AV) and *Atlantic Blue* (AB) polished limestone fragments subject to atmospheric conditions.

3.1. X-ray Fluorescence Spectrometry

Azul Valverde (references AV 27 and AV 43) and *Atlantic Blue* (AB 9 and AB 48) tiles 4X4 cm sized (Figure 4), both greyish polished limestones, were exposed to weathering in a rooftop terrace (Lisbon urban environment), subject to the normal atmospheric conditions (high UV radiation, low rainfall, wind, atmospheric pollution, and temperature changes, among others) for 3 months. The small square fragments were chemically checked for major, minor, and vestigial elements usually present in geological materials,

namely, Na, Mg, Al, Si, Cl, K, Ca, Ti, Mn, Fe, Zn, Rb, and Sr, in a weekly schedule (from May to July) and in the beginning of September 2016; a semi-quantitative analysis was performed through X-ray fluorescence spectrometry in wavelength dispersive mode (XRF-WDS) using a Philips PW1400 automated X-ray fluorescence spectrometer (50 kV, 45 mA) equipped with a rhodium tube and X-41 software. Fixed-time counts (5 × 30 s) were carried out over the diagnostic peaks of the selected elements and background, using the LiF200 analysing crystal for K, Ca, Ti, Mn, Fe, Zn, Rb and Sr, PET for Al, Si, and Cl, and PX-1 for Na and Mg.

3.2. X-ray Diffraction

A Philips PW 1500 powder diffractometer with Bragg–Brentano geometry, equipped with a large-anode copper tube operating at 50 kV–40 mA and a curved graphite crystal monochromator, was used to collect X-ray diffraction (XRD) patterns of the *Azul Valverde* (AV 27) and *Atlantic Blue* (AB 9) polished limestone fragments, before and after exposure to atmospheric conditions.

XRD was also performed on three areas of the *Azul Valverde* limestone fragment (Figure 5a)—yellow (reference AV Yellow (1) area), brown (AV Brown (2) area) and bluish-grey (AV Bluish-grey (3) area)—as well as in two other independent bluish-grey (AV Bluish-grey (A)) and yellow (AV Yellow (B)) fragments (Figure 5b) that were furthermore studied with synchrotron radiation (SR). A small quantity of powder from each area was used to obtain the XRD pattern. The photos of Figure 5 were taken under the same light intensity conditions to allow a better colour comparison.

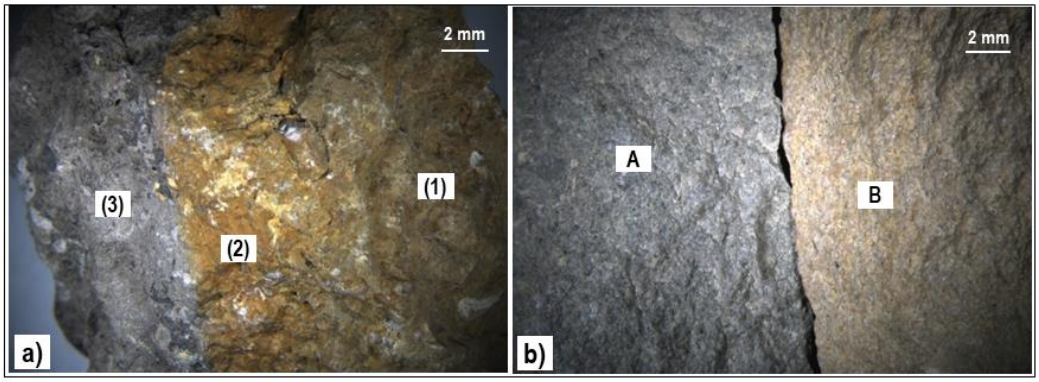

Figure 5. Images of the *Azul Valverde* limestone where the points studied with SR are assigned: (**a**) polychromatic fragment where the variation side by side between bluish-grey/brown/yellow is evident; (**b**) two independent bluish-grey and yellow fragments.

3.3. Scanning Electron Microscopy

A scanning electron microscope (SEM) Philips XL 30 FEG, with a field emission electron gun operated at an acceleration voltage of 10–20 kV under high vacuum, was used to study the morphology of the polished bluish-grey limestone fragments AV 27 and AB 9 before and after exposure to atmospheric conditions as well as to study a polished limestone fragment (from the Covão Alto quarry) with the two colours bluish-grey (AV Bluish-grey area) and yellow (AV Yellow area), side by side. Qualitative elemental analyses were performed with an energy dispersive X-ray spectrometer (EDS) coupled to the microscope. For the SEM/EDS analyses, the limestone fragments were coated with a thin layer of gold in a JEOL ion sputter JFC-1100 to improve the imaging capability. X-ray emission spectra were collected in spot mode analysis (around 3 nm beam resolution).

3.4. Colour Measurements

The colour measurements of the AB and AV stone slabs before (n = 3) and after exposition to weathering (n = 3) were performed with a CM-700d (Konica Minolta, Chiyoda

City, Japan) portable spectrophotometer. The measuring conditions were diameter viewing aperture of 10 mm, illuminant D65, and observer 10°. Measurements were performed on specular component excluded (SCE) mode excluding the specular component with open gloss trap (excluding most of the specular component). Calibration was performed with a black trap and white tile.

The CIELAB (CIE 1986) colour space was selected to represent the colour measurements the three coordinates: L* the lightness of the colour, which varies from 0 (black) to 100 (white); a* the redness (+)-greenness (-); and b* the yellowness (+)-blueness (-) [43]. The variation before and after ageing were assessed by calculating: the difference between the final and initial value of L* ($\Delta L^* = L^*_f - L^*_i$), a* ($\Delta a^* = a^*_f - a^*_i$), b* ($\Delta b^* = b^*_f - b^*_i$); Chroma ($C^*_{ab} = (a^* + b^*)^{1/2}$); and the total colour difference ($\Delta E^* = [(\Delta L^*)^2 + (\Delta a)^2 + (\Delta b)^2]^{1/2}$). Colour measurements have been often used to assess colour variations due to ageing and conservation treatments. In order to find significant differences, the measured L*, a*, and b* data were subjected to analysis of variance using Microsoft Excel 2010 for Windows. The averages were compared by the Tukey's honest significant difference (HSD) test at 5% level of significance.

3.5. Thermo-Analytical Techniques

Thermo-analytical assays—simultaneous differential thermal analysis (DTA) and thermogravimetry (TG)—were performed in unpolished *Azul Valverde* limestone, grey (AV Bluish-grey (A)), and yellow (AV Yellow (B)), for comparison purpose. A SETARAM 92–16.18 apparatus was used, incorporating a microbalance with a controlled argon gas flow. About 60 mg of milled and dried (about 2 h at 110 °C) sample was deposited in an alumina (Al_2O_3) crucible. The reference material was alumina powder. The heating temperature ranged from ambient to 1100 °C at a heating rate of 10 °C min^{-1}.

3.6. X-ray Absorption near Edge Structure and Energy Dispersive X-ray Fluorescence

Fe *K*-edge X-ray Absorption Near Edge Structure (XANES) spectra were collected in the unpolished *Azul Valverde* limestone fragment, namely, in the yellow (1), brown (2), and bluish-grey (3) zone [44], as well as in two other independent bluish-grey (A) and yellow (B) fragments (Figure 5). Model minerals were also studied by collecting XANES spectra in fluorescence yield (FY) mode using the instrumental set up of beamline BM 25A at the European Synchrotron Radiation Facility (ESRF) in Grenoble, France. XANES spectra were collected at the Fe *K*-edge (7112 eV) with an energy resolution of $\Delta E/E = 1.5 \times 10^{-4}$ using a 13-element Si(Li) solid-state detector (Sirius) and a Si(111) monochromator. An iron metal foil was irradiated for energy calibration purposes (first inflection point of the Fe *K*-edge set at 7112 eV). The chemical composition of the limestone samples was previously checked by energy dispersive X-ray fluorescence (EDXRF) using an excitation energy of 18 keV and an irradiated area of 1 mm^2. The high brilliance of synchrotron X-rays allows for remarkably low limits of detection for most chemical elements, thus enabling the analysis of trace and sub-trace species hosted by a mineral. The energy dispersive spectra collected for each sample were fitted using the PyMca software [45].

Iron model minerals were selected to configure different oxidation states and metal coordination, namely, ilmenite ($FeTiO_3$), pyrrhotite ($Fe_{1-x}S$), siderite ($FeCO_3$) and pyrite (FeS_2) for Fe^{2+} in octahedral coordination; hematite (α-Fe_2O_3), goethite [α-FeO(OH)], lepidocrocite [γ-FeO(OH)] and limonite [$FeO(OH).nH_2O$] for Fe^{3+} in octahedral coordination; magnetite (Fe_3O_4) for a mix of Fe^{2+} and Fe^{3+} in tetrahedral plus octahedral coordination.

XANES spectra were previously corrected in energy, the background was subtracted, and the spectra normalised for atomic absorption using the program Athena [46]. In addition to the experimental spectra collected for the model minerals, calculated spectrum for selected mixtures of minerals, including different ratios of mixtures, were also obtained by combination fitting method in Athena software, with the purpose to a better approach to the spectra collected on limestone fragments.

The details on the pre-edge region of the XANES spectrum (corresponding to the 1*s*→3*d* transition) have long been recognised as being mostly sensitive to the electronic structure and geometry of the iron site (e.g., [47]). The deconvolution of the pre-edge structure into pseudo-Voigt components using the program Fityk (2007) [48], a free software, to derive the height, energy position and total area (integrated intensity) of components, was used to assess the variation(s) in the electronic state(s) of iron in limestone. Thus, to extract the pre-edge features the contribution of the edge jump to the pre-edge was modelled using a spline function. The pre-edge features were then fit into pseudo-Voigt components (between 2 and 5) with a similar width [47,49]. Then, the total area (integrated intensity of all components) and the centroid position (intensity-weighted average of the component's positions) were calculated from the parameters of the fit.

4. Results and Discussion

4.1. Polished Limestone Exposed to Outdoor Atmospheric Conditions

4.1.1. Chemical and Mineralogical Characterization

The fixed-time counts after subtracting the background, obtained through XRF-WDS data, are compared for all elements except Ca (Figure 6), for better visualization. A high content of iron is visible in all fragments, and the presence of strontium is usually correlated to calcium content as known. Silicon is related to the presence of quartz, being higher in AB fragments. No significant chemical and mineralogical differences were observed for the *Azul Valverde* (AV) and *Atlantic Blue* (AB) polished limestone fragments when subject to outdoor atmospheric conditions; calcite is the main phase identified (Figure 7) with quartz and dolomite as vestigial phases, both before and after exposure.

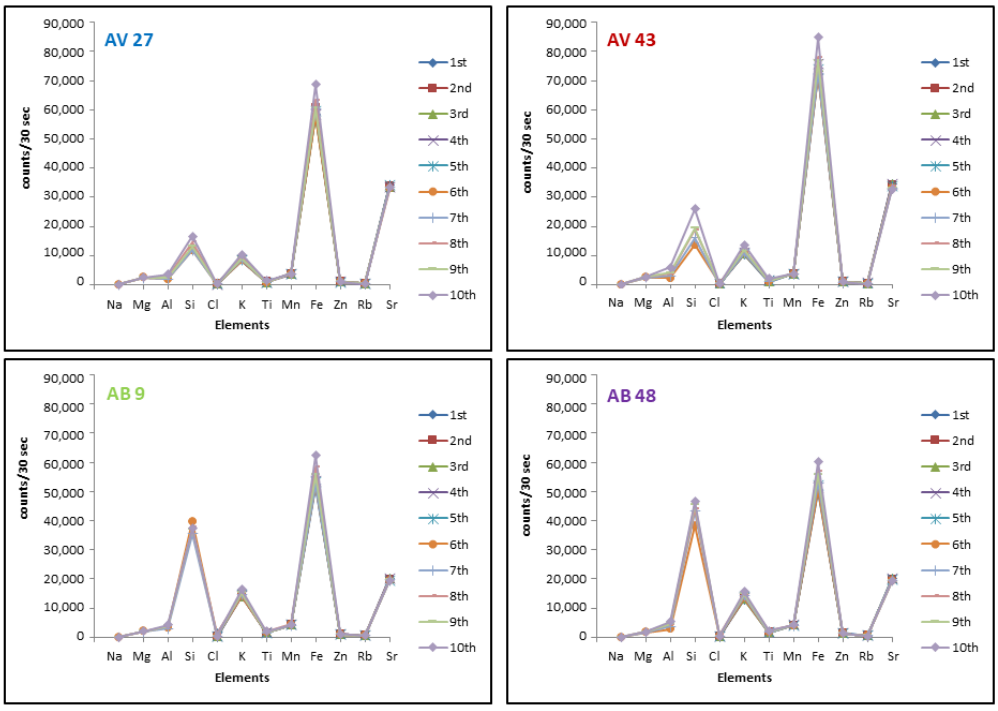

Figure 6. Plots of fixed-time counts variation along weeks (1st to 10th) for selected elements; *Azul Valverde* (AV) and *Atlantic Blue* (AB) polished limestone fragments.

Figure 7. Examples of XRD patterns of *Azul Valverde* (AV 27) and *Atlantic Blue* (AB 9) polished fragments, before and after exposure to outdoor atmospheric conditions; C—Calcite, $CaCO_3$ (JCPDS card number: 5-0586), D—Dolomite, $CaMg(CO_3)_2$ (11-78), Q—Quartz, α-SiO_2 (5-0490); the quartz peaks intensified by preferential orientation of the grains are assigned with an arrow ↑.

4.1.2. SEM Studies

Collected SEM images of *Azul Valverde* (Figure 8) before (a) and after (b) exposure, illustrate the morphology of polished limestone loosely suggesting higher roughness and/or porosity by the loss of material in the exposed fragment. Similarly, an alteration was observed in the *Atlantic Blue* (Figure 9a,b) where a smoothing of the grains seems to have occurred after exposure to outdoor atmospheric conditions (b); the bulk elemental constitution of both limestones is similar, the content of calcium is high and dominant, but small amounts of magnesium and silicon are also present. As expected, gold is present in all EDS spectra due to the coating of the sample. Quartz grains were also observed (Figure 9c,d) as displayed by the EDS spectrum. It should be noted that the value of open porosity for *Atlantic Blue* limestone, for instance, is considered low when compared to other limestones [50]; when subject to accelerated ageing tests, the limestone porosity increases slightly [50]. No microbial communities were detected by SEM.

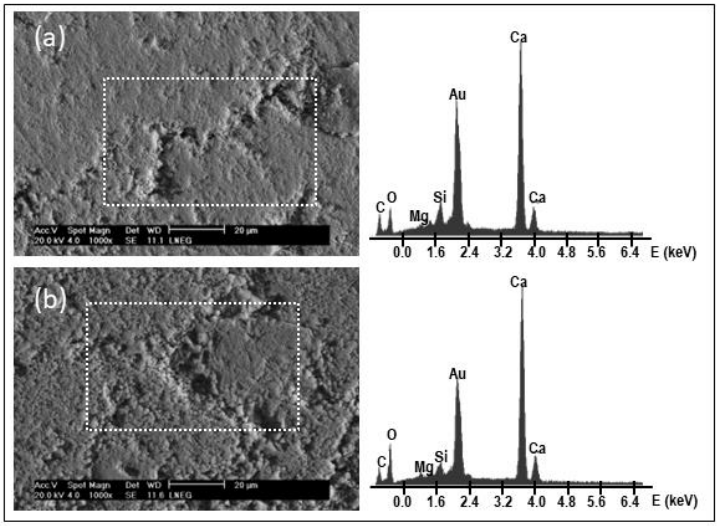

Figure 8. SEM images and EDS spectra, collected on the marked regions (white rectangles), of bluish-grey *Azul Valverde* polished limestone (AV 27), before (**a**) and after (**b**) exposure to atmospheric conditions; 1000X magnification.

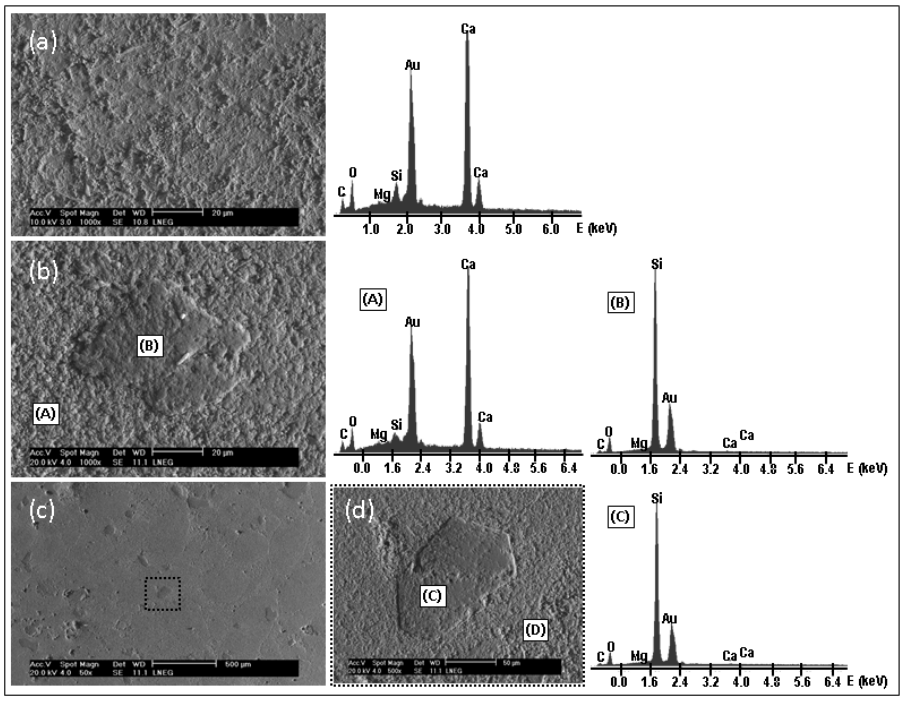

Figure 9. SEM images and EDS spectra of bluish-grey *Atlantic Blue* polished limestone (AB 9): (**a**) before exposure to outdoor atmospheric conditions (1000× magnification); (**b**) after exposure (1000×); (**c**) after exposure (50×); (**d**) detail of the selected area (500×), being spectrum (D) similar to (A).

4.1.3. Colour Fading

Near the smaller fragments (Figure 4) exposed to weathering in the rooftop terrace, entire tiles of AV and AB were also kept in similar conditions. For visual comparison, analogous entire tiles were also kept indoors, being photographed side by side at the end of the experiment as shown in Figure 10. Severe bleaching or fading [51] of the dark blue/greyish limestone was visually observed (Figure 10a), especially in the *Azul Valverde* samples after circa 3 months of exposure to sunlight, wind, rain, atmospheric pollution, and temperature changes among others, that cause weathering. Colour measurements confirm the chromatic alteration of the limestone slabs (see supplementary material Table S1). The *Azul Valverde* indeed showed a higher total colour variation ($\Delta E^* = 10.26$) than *Atlantic Blue* ($\Delta E^* = 3.28$). Both these values of ΔE^* are considered perceptible to the naked eye. The variation of the L value of *Atlantic Blue* was almost imperceptible, and values before and after exposure were not significantly different (Table S1). On both stones types a significantly different reduction of the C^*_{ab} (values of a* and b* decreased) was observed after weathering exposure (Figure 10b). The decrease of chroma value is one of the consequences of fading, as well as the increase of lightness value [52]. The increase of lightness was observed for *Azul Valverde*, causing a more severe bleaching effect when compared to *Atlantic Blue* limestone. In fact, colourimetry has been applied to study different materials, from the microelectronic field [53], to the Chinese blue-and-white archaeological porcelain [54], or even to the medieval tiles [55]. Furthermore, some authors have proposed a system for monitoring environmental conditions in museums based on the measurement of colour changes by image processing [56]. Colourimetry was also used to evaluate the colour and gloss of the original stones and to compare with those used in the restorations [10].

As already said, the exposure to atmospheric conditions results in stone ageing [9,10]. The summary of the atmospheric conditions [57] observed in the period of the limestone experiment (in the rooftop terrace) is shown in Table 2. As shown before, the time of exposition was not sufficient to promote any significant chemical, mineralogical, or structural modification, but fading was clearly visible. Indeed, the short wavelength of UV

radiation from sun often causes fading (e.g., [58]), and although this effect also occurs in a quarry, in a polished sample it is much more visible. The iron oxidation through UV radiation is an extremely rapid process [59,60], and this may have been the process that occurred with the polished limestone. In that sense, for buildings, works of art, or for decoration purposes in general, the grey natural stones must be correctly protected to minimise fading (see e.g., [11,12]).

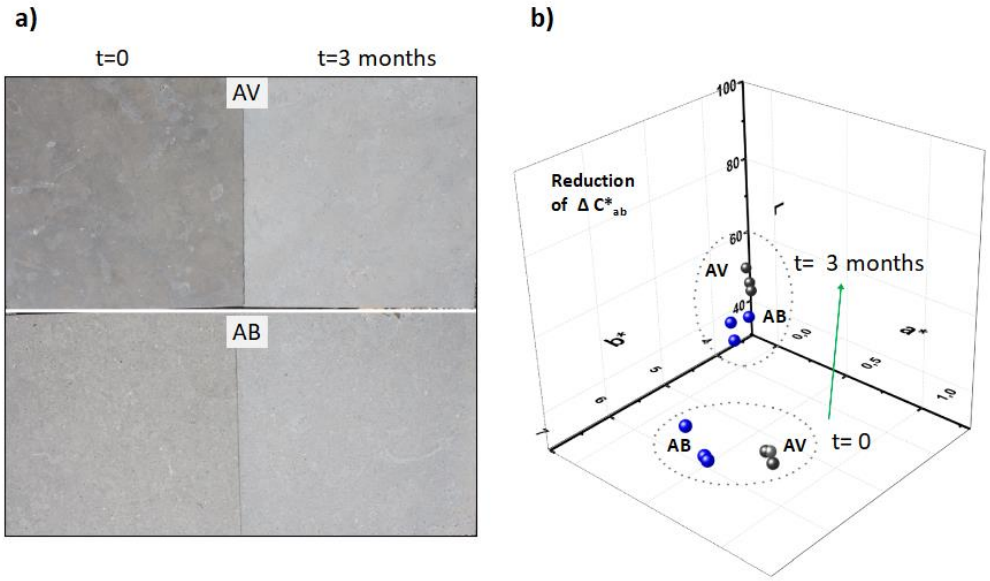

Figure 10. (**a**) Photography of the *Azul Valverde* (AV) and *Atlantic Blue* (AB) polished limestone tiles (30 × 30 cm), before (t = 0) and after (t = 3 months) being exposed to outdoor atmospheric conditions; (**b**) L* a* b* colour coordinate chart of samples AV and AB samples before (t = 0) and after (t = 3 months) being exposed to outdoor.

Table 2. Atmospheric conditions observed in Lisbon, during the experiment performed with polished limestone fragments subject to natural weathering, in 2016. Data from [57].

Month	Average Temperature, Minimum–Maximum (^{0}C)	Total Precipitation (mm)	Maximum Wind Intensity (Kmh^{-1})	Solar Irradiance (kWhm^{-2})
May	17.2, 11.1–30.8	133.4	65.2	>194
June	21.4, 14.1–34.0	1.4	61.9	>250
July	24.7, 15.0–36.5	0.0	65.2	>222
August	25.0, 16.4–36.6	0.0	59.0	>194

4.2. Colour Change in the Same Limestone Sample

4.2.1. Mineralogical Characterization

XRD patterns collected on the yellow, brown, and bluish-grey *Azul Valverde* limestone fragments (Figure 5) shows the presence of calcite as the main phase and quartz as a vestigial phase (Figure 11). Other vestigial phases are present, namely pyrite in the bluish-grey (3) and possibly goethite in brown (2); no further minerals that could be responsible for the colour of the limestone were identified.

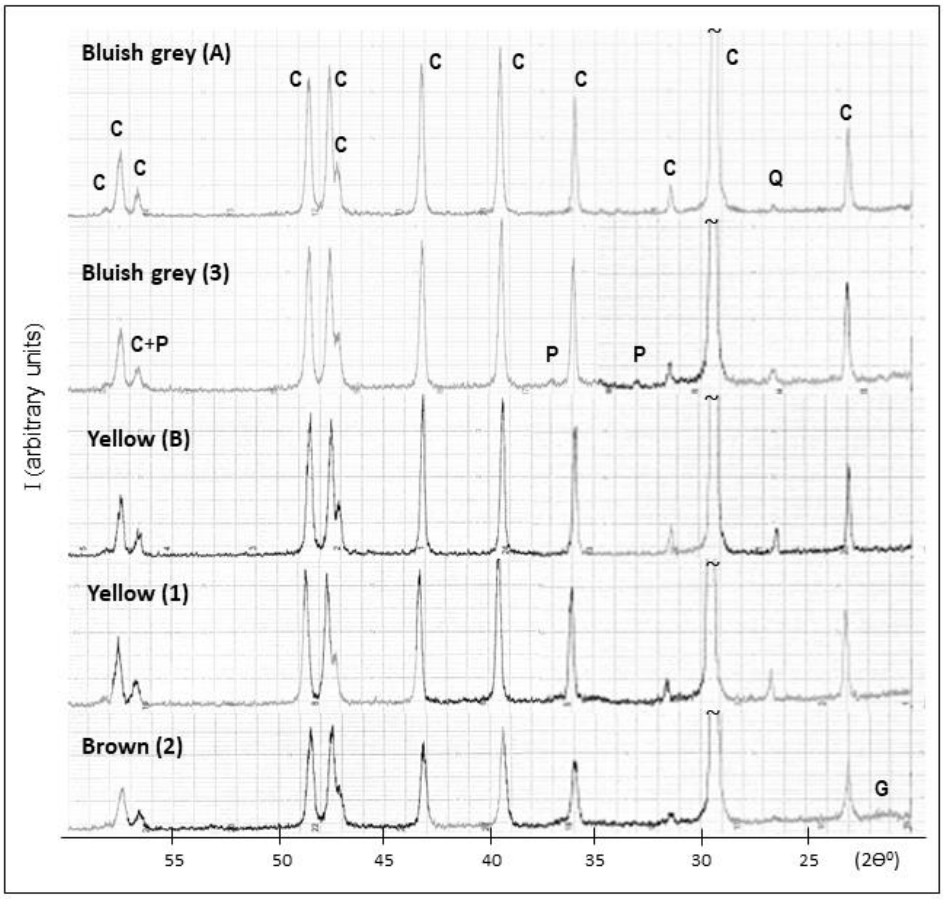

Figure 11. XRD patterns of *Azul Valverde* bluish-grey, yellow and brown uneven fragments; C—Calcite, $CaCO_3$ (JCPDS card number: 5-0586), G—Goethite, α-FeO(OH) (17-536), P—Pyrite, FeS_2 (6-0710); Q—Quartz, α-SiO_2 (5-0490).

4.2.2. SEM Studies

SEM images of the *Azul Valverde* polished polychromatic limestone fragment are compared in Figure 12, for the yellow (a) and for the bluish-grey (b) areas side by side. The EDS spectra are very similar in both colours and the presence of aluminium, potassium, and iron, although in a very low content, suggest the occurrence of additional phases such as feldspars and iron oxides. Comparatively, when the fragments are only bluish-grey as was the case of *Azul Valverde* and *Atlantic Blue* samples (Figures 8 and 9), those elements are not detected, suggesting that polychromatic limestone correspond to a transition zone due to fluid percolation.

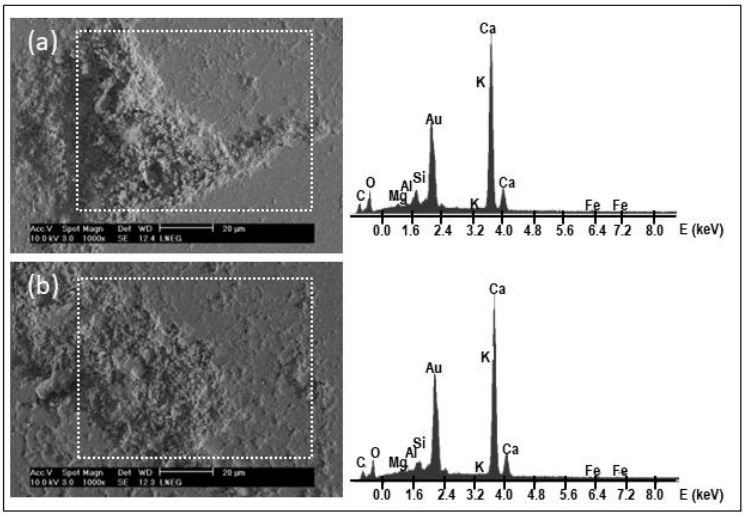

Figure 12. SEM images and EDS spectra, collected on the marked regions (white rectangles), of *Azul Valverde* polished polychromatic limestone fragment from Covão Alto quarrying area (1000× magnification): (**a**) yellow area; (**b**) bluish-grey area.

4.2.3. DTA–TG Assays

The DTA–TG curves obtained for grey (AV Bluish-grey (A)) and yellow (AV Yellow (B)) *Azul Valverde* limestone (Figure 13) were compared to published data [61] (p. 108) and the phase constitution of heated material was monitored by XRD. One endothermic peak, due to the decomposition of calcite under inert atmosphere, was obtained at 925 °C (grey) and 931 ˚C (yellow) and CaO was the resulting material. The mass loss was 42.70% for the grey sample and 43.85% for the yellow one, very close to the theoretical value of 44%. The small differences found could be related to the presence of vestigial phases such as quartz or dolomite, or even alkali salts [62]. Furthermore, the two little endothermic peaks between 600–700 °C in the bluish-grey sample (Figure 13a), could be attribute to the dissociation of pyrite to pyrrhotite [61] (p. 53).

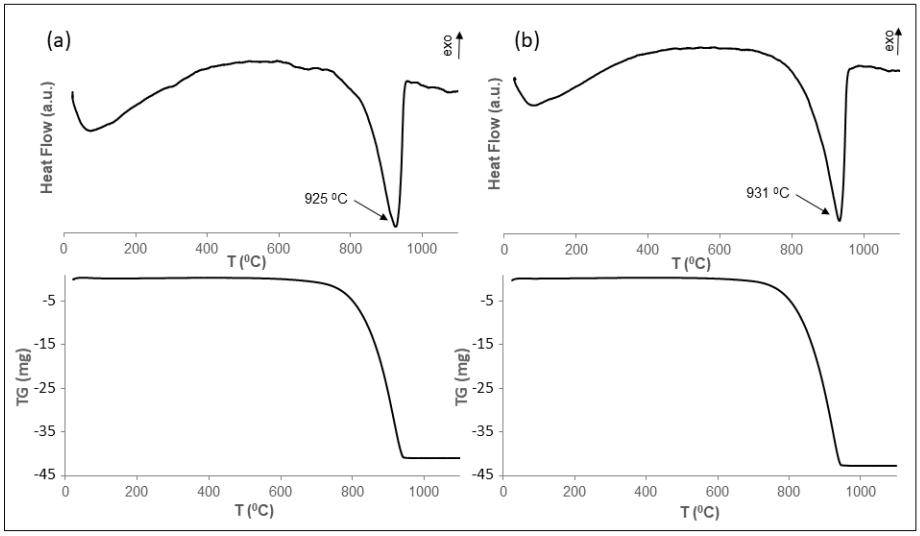

Figure 13. DTA–TG heating curves of *Azul Valverde* limestone: (**a**) AV Bluish-grey (A); (**b**) AV Yellow (B).

4.2.4. Iron Speciation

The qualitative chemical composition of the *Azul Valverde* limestone sample (Figure 14) was also checked in three points, one in each coloured area (Figure 5), by EDXRF with synchrotron radiation; however, for some reason, the yellow area had less fluorescence signal. Comparatively, the brown and bluish-grey zones are chemically similar, but the brown zone has an increment in the iron content relatively to the bluish-grey. Sulphur is present, but the peak is overlaid with the escape peak of calcium. Argon is from the instrumental set up of the beamline and not from the sample.

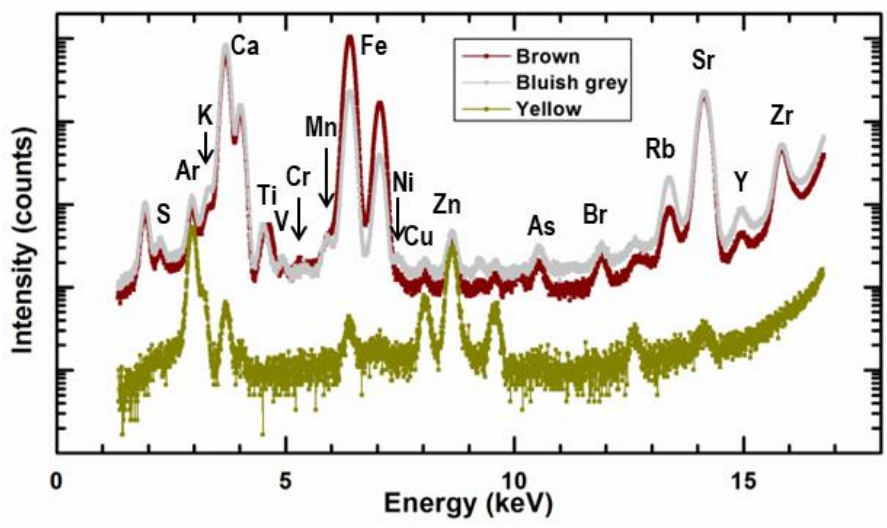

Figure 14. EDXRF spectra of coloured limestone areas obtained with excitation energy of 18 keV. The intensity of the peaks close to the excitation energy is increased. Only the diagnostic peak ($K\alpha$) of each element is assigned.

X-ray absorption spectroscopy is a powerful tool of assessing the formal valence of cations (particularly transition metal ions) and their coordination environment. The near-edge features of XANES spectra provide information about the speciation of the absorbing element—that is, its oxidation state and coordination geometry; for 3*d* transition metal ions, the interval of 15-20 eV before the main *K*-edge crest discloses details related to 1*s*→3*d* (quadrupolar) and/or 1*s*→4*p* (dipolar) electronic transitions [47,63].

For the Fe *K*-edge XANES spectra (Figure 15) obtained in the yellow (1), brown (2), and bluish-grey (3) area of the *Azul Valverde* limestone fragment (Figure 5), the main crest was assigned at 7131 eV for the first two and at 7133 eV for the last one. The post-edge details (a, b, and c) are in the same energy position for both brown (2) and yellow (1) spectra; conversely, bluish-grey (3) spectrum display small differences in energy position and an intensity of detail b lower than c. For the two independent fragments, yellow (B) and bluish-grey (A), the main crest energy position was observed at 7133 eV. The intensity of details b and c are slightly different, being bluish-grey (A) and similar to bluish-grey (3). The energy position of the pre-edge is around 7114.5 eV in all samples. *K*-edge energy position (Figure 16) varies between bluish-grey samples (7119 eV, achieved through the first derivative) to brown sample (7124 eV), suggesting the predominance of Fe^{2+} oxidation state in the first ones and Fe^{3+} in the last one (e.g., [64]).

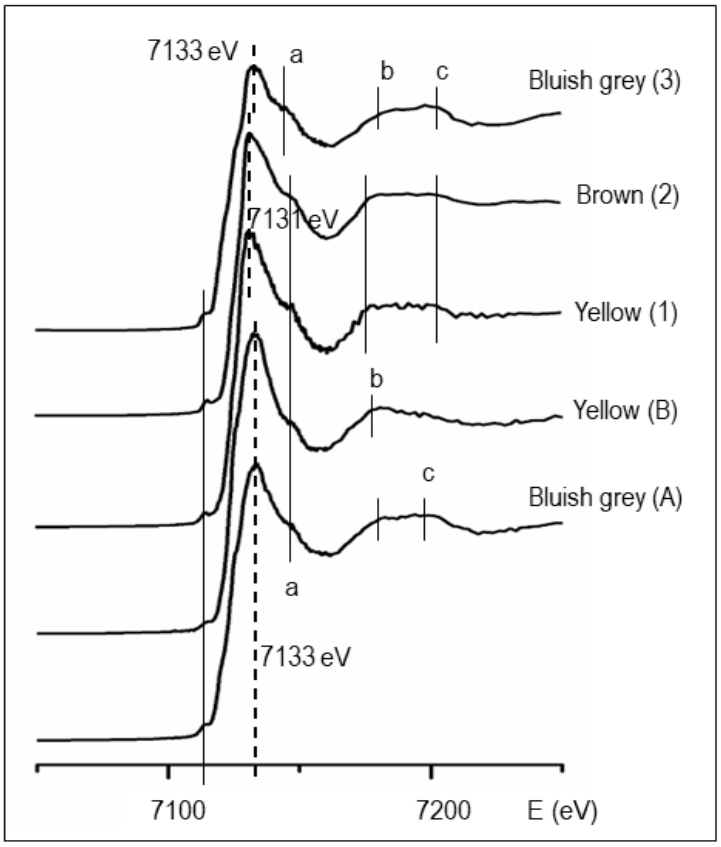

Figure 15. Normalised Fe *K*-edge XANES spectra of the *Azul Valverde* limestones collected in the three coloured zones side by side and in the two independent fragments (A and B), shown in Figure 5. The solid and dashed lines, indicates the position of the pre-edge and main crest, respectively. Post-edge details (a–c) are also assigned.

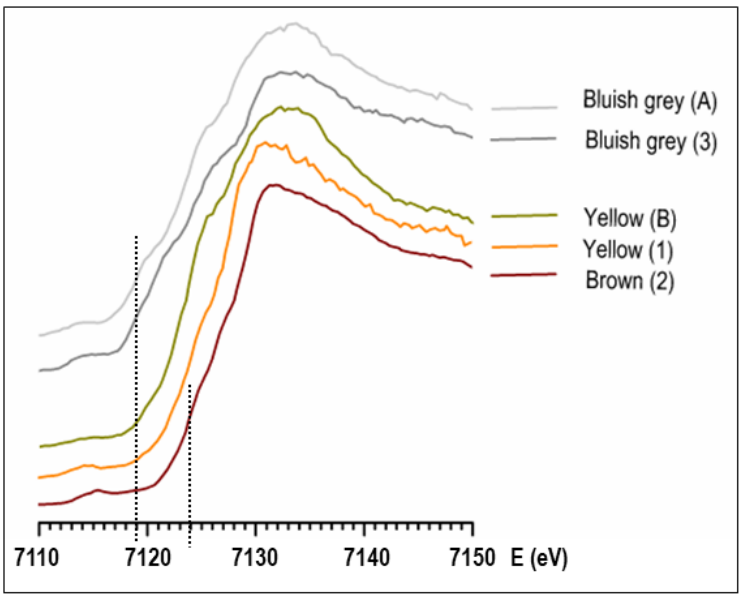

Figure 16. Energy variation of iron *K*-edge for *Azul Valverde* limestone samples. The energy position of the *K*-edge for the bluish-grey and brown samples is assigned.

However, pre-edge energy position and intensity are more sensitive to iron oxidation state and coordination geometry [65]. The pre-edge can be fitted in pseudo-Voigt

components that are related to metal electronic transitions, mainly 1*s*→3*d*. Depending on the oxidation state and electronic coordination (octahedral, tetrahedral, or square pyramidal) the number of components can change in agreement with theoretical predictions [66]. For 4-coordinated Fe^{2+} (tetrahedral), the crystal-field theory predicts four transitions [47,63]. In the same way, for 6-coordinated Fe^{2+} (octahedral), three components are predicting, but if site distortion occurs in the regular octahedron only two maxima are distinguishable. The intensity of the pre-edge lowers with the increase of the extent of centro-symmetry geometry as observed for ferrous minerals in tetrahedral coordination. For octahedrally coordinated Fe^{3+} minerals, two components plus one to three extra components could be observed. The extra components are related to long-range order between Fe–Fe pairs, involving 3*d* orbitals [67].

The deconvolution of the pre-edge spectra achieved for all iron model minerals are compared in Figure 17. Additionally to the spectra of model minerals collected in beamline BM 25A, some spectra former acquired in beamline ID 21 were also added, namely: bornite (Cu_5FeS_4), carrollite ($CuCo_2S_4$, where Fe substitutes Cu) and chalcopyrite ($CuFeS_2$) for Fe^{2+} in tetrahedral coordination; and copiapite [$(Fe^{2+})^o(Fe^{3+})^o_4(SO_4)_6(OH)_2.20H_2O$] for Fe^{2+} and Fe^{3+} in octahedral coordination.

As expected, an energy shift of the centroid to higher energies, is verified from Fe^{2+} to Fe^{3+}. For ferrous minerals, the centroid energy varies between siderite and pyrite, followed by the minerals with a mix of Fe^{2+} and Fe^{3+}, and finally the ferric ones with higher energies. The energy of the centroid (dash-dot line), calculated with the relative height and energy of each contribution [47] is assigned.

The same treatment was performed for the pre-edges of limestone samples and the results of the total area (integrated intensity of all components) versus centroid position, for model minerals plus samples, are plotted in Figure 18. As already mentioned, the pre-edge position shifts towards higher energy with increasing oxidation state. The intensity of the pre-edge is inversely correlated with the extent of centro-symmetry of the crystallographic site of Fe [47], that means that higher intensity is predictable when Fe^{2+} is 4-coordinated (tetrahedral); indeed, the total area achieved by the pre-edges of chalcopyrite, carrollite and bornite (the three more intense Fe^{2+} minerals) reflects this fact. Bluish-grey samples are roughly located near the 6-coordinated (octahedral) ferrous model minerals and the brown limestone in the zone of higher energy, near the ferric minerals. In the intermediate zone, are placed the yellow samples, as well as the minerals with mixed valence for iron.

The fitting of the pre-edge spectra obtained on the bluish-grey samples (three components) and the centroid energy are similar to that of the pyrite (Figure 19); indeed, for 6-coordinated Fe^{2+} minerals, the spectrum must be fitted with three components, in agreement with theoretical predictions (or two if site distortion occurs) [47]. However, the intensity of the pre-edge is similar to pyrrhotite, probably due to a mixture of these two minerals in the bluish-grey samples. In the same way, in the brown sample, a 6-coordinated Fe^{3+} seems to be present, being the intensity and centroid position similar to goethite; in this case, two principal components were foreseen, plus one to three extra components [47]. The yellow samples are probably a mixture of Fe^{2+} and Fe^{3+}.

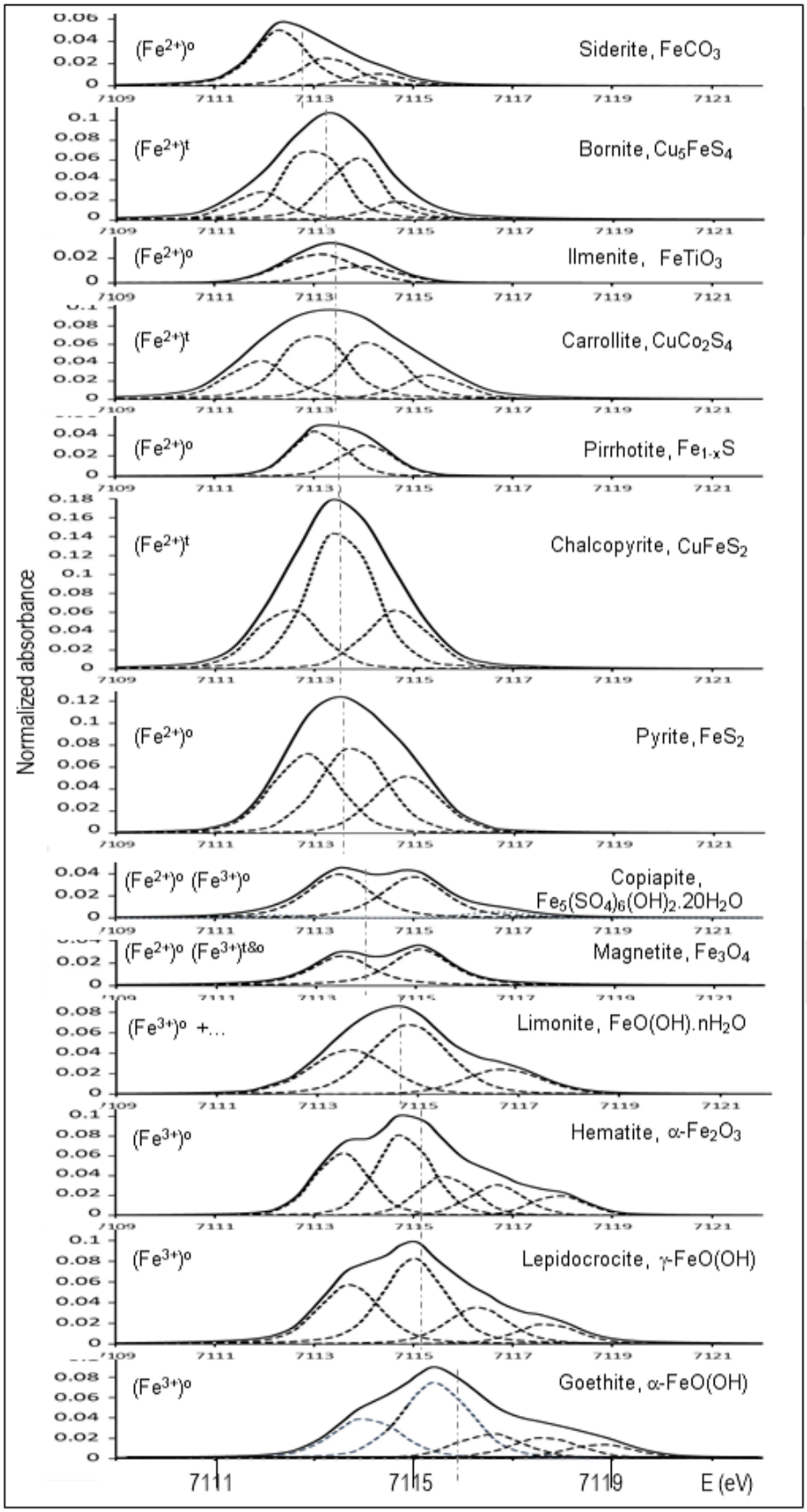

Figure 17. Normalised pre-edge spectra (Fe *K*-edge) obtained for Fe^{2+} and Fe^{3+} model minerals including that with mixing valences (o-octahedral and t-tetrahedral coordination). The energy of the centroid (dash-dot line) is assigned.

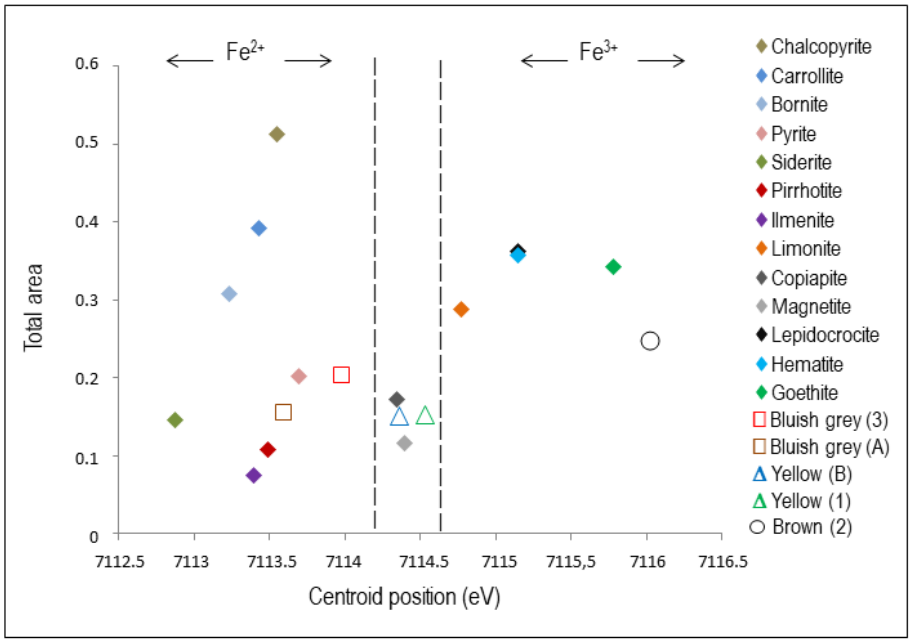

Figure 18. Total area vs. centroid position for pre-edges deconvolution: diamond—model minerals; square—bluish-grey, triangle—yellow and circle—brown limestone.

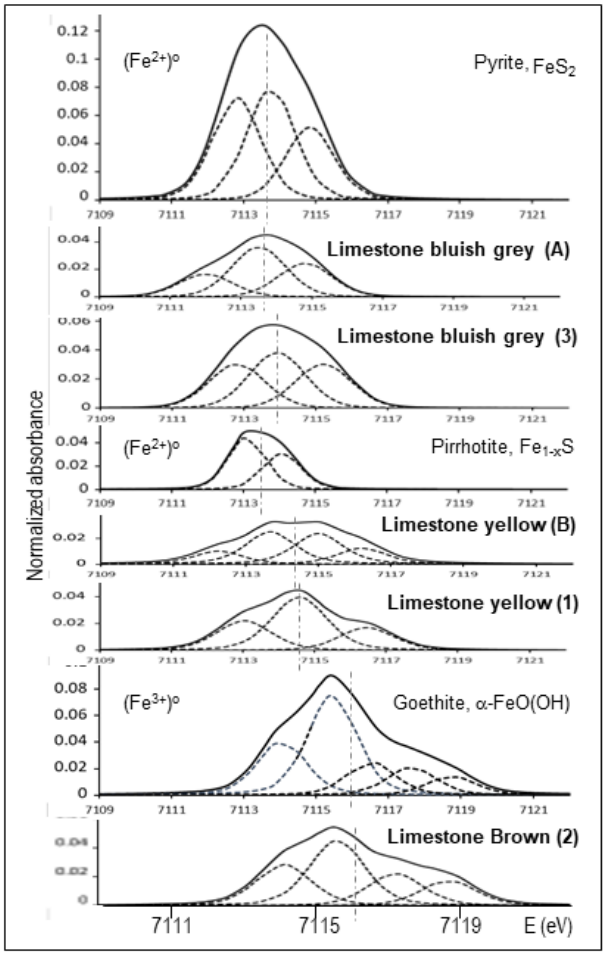

Figure 19. Normalised pre-edge spectra (Fe *K*-edge) and the best model calculated (using Fityk program). The centroid is assigned with a dash-dot line.

The comparison of XANES details including the main crest between bluish-grey samples and standards with 6-coordinated Fe^{2+} (namely pyrite and pyrrhotite) was performed (Figure 20). In addition to the experimental spectra of the model minerals, calculated spectra were also obtained. In fact, the calculated spectra for mixtures of pyrite and pyrrhotite, considering the ratio 1:1 and 2:1, respectively, led us to suppose that in the bluish-grey samples both pyrite and pyrrhotite are present, probably in a ratio of 2:1, as the energy position and intensity of the details are similar to the spectrum 2xPyrite + Pyrrhotite. The difference in the main crest intensity observed in the samples, is explained by the superficial oxidation of the minerals. Previous studies on unoxidised, slightly oxidised, and heavily oxidised pyrites showed differences on XANES spectra, namely in the pre-edge region and main crest [68] (Figure 2). The pre-edge region is largest in the least oxidised sample and decreases with increasing degree of oxidation; the changes in the remaining features exhibit a progression from unoxidised pyrite to the most highly oxidised sample, reflecting the development on the surface of a phase with spectral characteristics similar to those of goethite [68]. In the same way, considering the XANES spectrum of the brown limestone sample compared to the 6-coordinated Fe^{3+} model mineral, goethite, a similar trend (spectrum details and main crest) was observed. For the yellow samples, the details and main crest of the spectra are similar to the calculated spectrum of goethite plus pyrite in a ratio of 10:1. Keeping in mind the contribution of organic matter to this subject, the change on the limestone colour can also be explained by the presence of small quantities of iron, being Fe^{2+} responsible for the grey and Fe^{3+} for the yellow/brown [69]; alkaline fluids were responsible for the pyrite oxidation probably giving rise to the formation of goethite (e.g., [68,70]). In fact, the surface oxidation products of pyrite vary with pH, with a marked transition occurring around pH 4, in aqueous air-saturated solutions, as observed by some authors [70]. They found that under alkaline conditions, the surface oxidation layer consists only of Fe^{3+} oxyhydroxide (probably goethite). Experiments performed by Bladh [71] on the weathering of iron sulphide-bearing felsic rocks shown that goethite is usually the first mineral containing ferric ion that forms during weathering. The presence of iron in the form of ferric iron, Fe^{3+} and ferrous iron, Fe^{2+} influences strongly the hue and durability of the stone being limestone's colour related to the FeO/Fe_2O_3 ratio [57]. Studies regarding the genesis of carbonate breccia in South Korea [40] revealed that the greyish matrix breccia consists mainly of calcite and dolomite, and minor quartz and pyrite and the yellowish part consists of pyrite that was oxidised to goethite or iron oxi-hydroxides.

Research on Lower Globigerina Limestone from Malta pointed out that oxidation during the process of fragmentation might have changed the limestone colour from an original bluish-grey to yellow and ochre-brown as colour is caused by oxidizing or reducing processes at the time of sedimentation [72]. The limestone colour changed from bluish-green to yellow due to post-depositional oxidation resulting from water flowing through the cracks (ferric solutions). Furthermore, that findings pointed to the usual instability of the iron hydroxides or limonite minerals (pigments) if exposed to light and weathering, and to a reasonable correlation of colour with the Fe_2O_3 content. Concerning the results obtained in the present study and in a broad way, when Fe^{2+} content >> than Fe^{3+}, the limestone is dark (bluish-grey); when Fe^{2+} content << than Fe^{3+}, the limestone is yellow or brown (see Figure 5a).

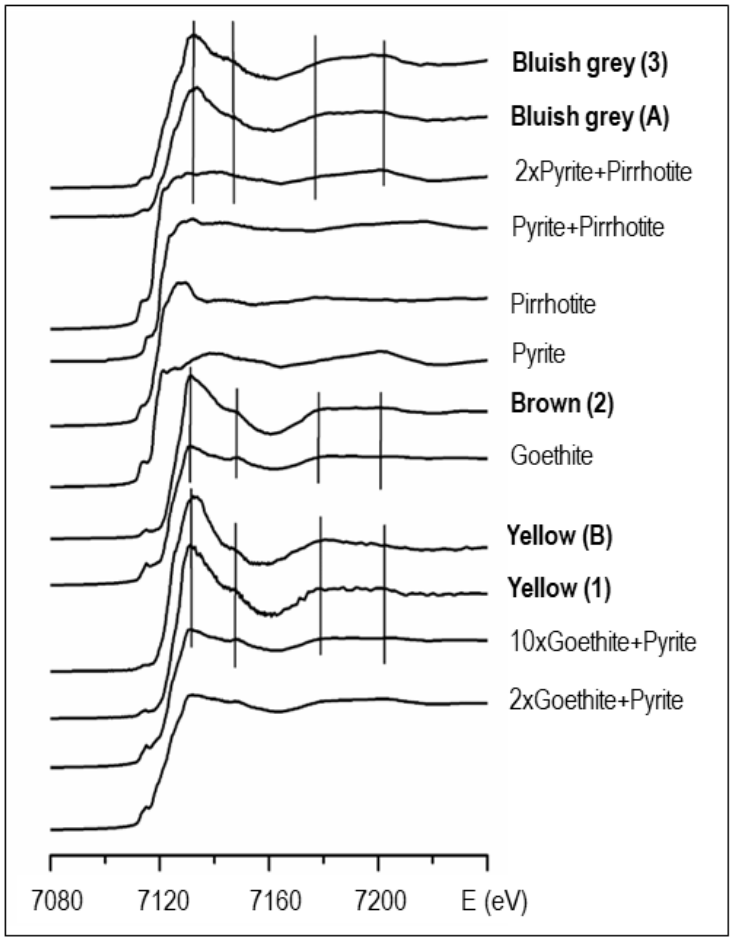

Figure 20. Normalised Fe *K*-edge XANES spectra of bluish-grey limestone samples compared to the experimental spectra of model minerals and to calculated spectra for the mixtures of minerals.

5. Conclusions

The change of colour observed in bluish-grey limestones, namely, *Azul Valverde* and *Atlantic Blue* samples, which are important ornamental stones in buildings, but used in works of art as well, can be explained through the following factors:

(1) The UV radiation from the sun causes quick and severe bleaching or fading process on the dark blue/grey polished limestone placed outdoor during circa 3 months (natural weathering), visible to the naked eye; the presence of sulphates or microbial communities commonly associated to the weathering of the limestone were not detected.

(2) The presence of small quantities of Fe^{2+} and Fe^{3+} are responsible for the greyish and yellow/brown colour side by side in the same limestone sample, respectively; the study performed with synchrotron radiation (XANES) allowed us to disclose the iron speciation, by comparison to model minerals and also by deconvolution of the pre-edge structure into pseudo-Voigt components. The iron model minerals were selected to configure different oxidation states and metal coordination. The evaluation with calculated spectra, allowed us to conclude that in the bluish-grey limestone, both pyrite and pyrrhotite in a proportion of 2:1 are present, while in brown and yellow limestone, goethite is possibly present. Although, in the yellow limestone, a mixture of goethite and pyrite in a ratio of 10:1 was noticed. Indeed, the pyrite oxidation most likely gives rise to the formation of goethite by percolation of alkaline fluids that was probably the mechanism responsible for the sudden variation of colour side by side.

In fact, fading is possibly the first weathering effect that occurs. While this effect also happens in a quarry, it is much more visible in a polished sample. Both the UV radiation and the percolation of alkaline fluids could give rise to the pyrite oxidation. In that sense, for the preservation of the built heritage, for works of art, or even for decoration purposes in general, the limestone surfaces must be protected with adequate coatings to minimise the iron oxidation in the bluish-grey natural stones, as this is considered unaesthetic.

Author Contributions: Conceptualization, T.P.S., D.d.O. and J.P.V.; methodology, T.P.S., J.P.V., M.A.B., M.L.C. and E.S.-C.; investigation, T.P.S., D.d.O., J.P.V., V.L. and J.C.; writing—original draft preparation, T.P.S., D.d.O., J.P.V., V.L. and J.C.; writing—review and editing, T.P.S., D.d.O., J.P.V., V.L., J.C., M.A.B., M.L.C., E.S.-C. and R.V.; visualization, T.P.S.; funding acquisition, M.L.C. and J.P.V. All authors have read and agreed to the published version of the manuscript.

Funding: M.L. Coutinho acknowledges FCT-Portuguese Foundation for Science and Technology for contracts CEECIND/00349/2017, UIDB/04449/2020 and UIDP/04449/2020. J.P. Veiga acknowledges FEDER funds through the COMPETE 2020 Programme and National Funds through FCT-Portuguese Foundation for Science and Technology under the project ref. UIDB/50025/2020-2023 and funding from the European Institute of Innovation and Technology (EIT), a body of the European Union, under Horizon 2020, the EU Framework Programme for Research and Innovation, through the MineHeritage Project (PA 18111).

Acknowledgments: MVC-Mármores de Alcobaça is thanked for supplying samples for this study. The authors acknowledge the European Synchrotron Radiation Facility for provision of synchrotron radiation facilities and in particular in using beamlines BM 25A (experiments HG-100 and HG-118) and ID 21 (ME-821 and EC-87). Special thanks are due to the colleague João Fernandes for helping in the plots of fixed-time counts. Fundação Bragança is also acknowledged for the images of the façade before and after conservation and restoration intervention. The authors are also grateful to the anonymous reviewers and editors for their comments on the manuscript.

Conflicts of Interest: The authors declare no conflict of interest.

References

1. Clemente, I.M.; Artur, A.C.; Neto, J.A.N. Image analysis in the evaluation of chemical attack on carbonate rocks of Potiguar and Araripe basins. *Est. Geol.* **2013**, *23*, 29–44. (In Brazilian Portuguese)
2. Marie, I. Perception of darkening of stone facades and the need for cleaning. *Int. J. Sustain. Built Environ.* **2013**, *2*, 65–72. https://doi.org/10.1016/j.ijsbe.2013.09.001.
3. Perez-Monserrat, E.M.; Fort, R.; Varas-Muriel, M.J. Monitoring façade soiling as a maintenance strategy for the sensitive built heritage. *Int. J. Archit. Hérit.* **2018**, *12*, 816–827. https://doi.org/10.1080/15583058.2017.1419312.
4. Thornbush, M.; Viles, H. Integrated digital photography and image processing for the quantification of colouration on soiled limestone surfaces in Oxford, England. *J. Cult. Hérit.* **2004**, *5*, 285–290. https://doi.org/10.1016/j.culher.2003.10.004.
5. Columbia Stone, 2008. Available online: http://www.columbiastone.com/portfolio/wsu-compton-union-building-cub-renovation/ (accessed on 16 April 2022).
6. JMU Centennial Celebration, The History of Bluestone, 2020. Available online: https://www.jmu.edu/centennialcelebration/bluestone.shtml (accessed on 16 April 2022).
7. Albert, J. 2014. Natural Stone: Problems and Solutions for the Use in Outdoor Areas. *LitosOnLine.com*, 121. Available online: https://www.litosonline.com/en/article/natural-stone-problems-and-solutions-use-outdoor-areas (accessed on 16 April 2022).
8. Casal Moura, A. *Ornamental Marbles and Limestones of Portugal;* Gestão de Artes Gráficas, SA: Amadora, Portugal, 2007; p. 383. (In Portuguese)
9. González-Avilés, A.B.; Echarri-Iribarren, V.; Galiano-Garrigós, A.; Rizo-Maestre, C.; Pérez-Millán, M.I. Colour Ageing in Acrylic Resin Plates and Natural Minerals on the Façade after 10 Years of Sun Exposure in the Marine Environment. *Appl. Sci.* **2021**, *11*, 2222. https://doi.org/10.3390/app11052222.
10. Ribeiro, R.C.C.; Figueiredo, P.M.F.; Barbutti, D.S. Multi-Analytical Investigation of Stains on Dimension Stones in Master Valentim's Fountain, Brazil. *Minerals* **2018**, *8*, 465. https://doi.org/10.3390/min8100465.
11. Aldoasri, M.A.; Darwish, S.S.; Adam, M.A.; Elmarzugi, N.A.; Ahmed, S.M. Enhancing the Durability of Calcareous Stone Monuments of Ancient Egypt Using $CaCO_3$ Nanoparticles. *Sustainability* **2017**, *9*, 1392. https://doi.org/10.3390/su9081392.
12. Pargoletti, E.; Comite, V.; Fermo, P.; Sabatini, V.; Cappelletti, G. Enhanced Historical Limestone Protection by New Organic/Inorganic Additive-Modified Resins. *Coatings* **2021**, *11*, 73. https://doi.org/10.3390/coatings11010073.
13. Siegesmund, S.; Snethlage, R. *Stone in Architecture—Properties, Durability*, 4th ed.; Springer-Verlag: Berlin, Germany, 2011; p. 552.

14. Smith, B.; Viles, H.A. Rapid, catastrophic decay of building limestones: Thoughts on causes, effects and consequences. In *Heritage Weathering and Conservation*; González, R.F., De Buergo, M.A., Gómez-Heras, M., Eds.; Taylor and Francis: Abingdon, UK, 2006; Volume 1, pp. 531–537.
15. Myrow, P.M. A new graph for understanding colors of mudrocks and shales. *J. Geol. Educ.* **1990**, *38*, 16–20. https://doi.org/10.5408/0022-1368-38.1.16.
16. Dias, L.; Rosado, T.; Coelho, A.; Barrulas, P.; Lopes, L.; Moita, P.; Candeias, A.; Mirão, J.; Caldeira, A.T. Natural limestone discolouration triggered by microbial activity—A contribution. *AIMS Microbiol.* **2018**, *4*, 594–607. https://doi.org/10.3934/microbiol.2018.4.594.
17. Azerêdo, A.C.; Mendonça Filho, J.G.; Cabral, M.C.; Duarte, L.V. Pedogenic limestones and organic-matter rich levels in the Middle Jurassic from Pedreira do Galinha, Serra de Aire: A multidisciplinary approach. *Comum. Geol.* **2013**, 100, 95–100. (In Portuguese)
18. Pires, V.; Amaral, P.M.; Simão, J.A.R.; Galhano, C. Experimental procedure for studying the degradation and alteration of limestone slabs applied on exterior cladding. *Environ. Earth Sci.* **2022**, *81*, 59. https://doi.org/10.1007/s12665-022-10204-3.
19. Santos, M.A.C. Mechanisms of Discoloration of the "Blue" Limestone from "Maciço Calcário Estremenho". Unpublished MSc Thesis, Sciences Faculty, Lisbon University: Lisbon, Portugal, 2017. (In Portuguese)
20. Bams, V.; Dewaele, S. Staining of white marble. *Mater. Charact.* **2007**, *58*, 1052–1062. https://doi.org/10.1016/j.matchar.2007.05.004.
21. Cucci, C.; De Pascale, O.; Senesi, G.S. Assessing Laser Cleaning of a Limestone Monument by Fiber Optics Reflectance Spectroscopy (FORS) and Visible and Near-Infrared (VNIR) Hyperspectral Imaging (HSI). *Minerals* **2020**, *10*, 1052. https://doi.org/10.3390/min10121052.
22. Binal, A.; Ayderman, A.; Sel, A. Colour Changes on the Surface of the Rock Materials Due to UV-A and UV-B Rays. *Geophys. Res. Abstr.* **2015**, *17*, EGU2015-1447-2.
23. Worthington, S. Does Natural Stone Fade? Understanding Colour in Stone, AquaMix Australia. 2015. Available online: https://aquamix.com.au/reference-library/technical-articles/does-natural-stone-fade/ (accessed on 19 May 2022).
24. Careddu, N.; Marras, G. The effects of solar UV radiation on the gloss values of polished stone surfaces. *Constr. Build. Mater.* **2013**, *49*, 828–834. https://doi.org/10.1016/j.conbuildmat.2013.09.010.
25. Figueiredo, M.O.; Silva, T.P.; Veiga, J.P. Ancient glazed ceramic tiles: A long-term study from the remediation of environmental impacts to the non-destructive characterization of materials. In Proceedings of the International Seminar on Conservation of Glazed Ceramic Tiles: Research and Practice, Lisbon, Portugal, 15–16 April 2009; CDROM, p. 10.
26. Rosado, T.; Dias, L.; Lança, M.; Nogueira, C.; Santos, R.; Martins, M.R.; Candeias, A.; Mirão, J.; Caldeira, A.T. Assessment of microbiota present on a Portuguese historical stone convent using high-throughput sequencing approaches. *MicrobiologyOpen* **2020**, *9*, 1067–1084. https://doi.org/10.1002/mbo3.1030.
27. Dias, L.; Rosado, T.; Candeias, A.; Mirão, J.; Caldeira, A.T. A change in composition, a change in colour: The case of limestone sculptures from the Portuguese National Museum of Ancient Art. *J. Cult. Hérit.* **2020**, *42*, 255–262. https://doi.org/10.1016/j.culher.2019.07.025.
28. Wilson, R.C.L.; Hiscott, R.N.; Willis, M.G.; Gradstein, F.M. The Lusitanian Basin of west-central Portugal: Mesozoic and Tertiary tectonic, stratigraphic, and subsidence history. In *Extensional Tectonics and Stratigraphy of the North Atlantic Margins*; Tankard, A.J., Balkwill, H.R., Eds.; AAPG: Tulsa, OK, USA, 1989; pp. 341–361.
29. Ribeiro, A.; Silva, J.B.; Cabral, J.; Dias, R.; Fonseca, P.; Kullberg, M.C.; Terrinha, P.; Kullberg, J.C. Tectonics of the Lusitanian Basin. In *Final Report, Project MILUPOBAS, EC-Contract nº JOU-CT94-0348, ICTE/GG/GeoFCUL*; Lisbon University: Lisbon, Portugal, 1996; p. 126.
30. Pinheiro, L.M.; Wilson, R.C.L.; Pena Dos Reis, R.; Whitmarsh, R.B.; Ribeiro, A. The western Iberia margin: A geophysical and geological overview. In *Proceedings of the Ocean Drilling Program, Scientific Results, Balboa, Panama, 16 October–17 December 1996*; Whitmarsh, R.B., Sawyer, D.S., Klaus, A., Masson, D.G., Eds.; TX (Ocean Drilling Program): College Station, TX, USA, 1996; pp. 1–23.
31. Kullberg, J.C.; Rocha, R.B.; Soares, A.F.; Rey, J.; Terrinha, P.; Azerêdo, A.C.; Callapez, P.; Duarte, L.V.; Kullberg, M.C.; Martins, L.; et al. A Bacia Lusitaniana: Estratigrafia, Paleogeografia e Tectónica. In *Geologia de Portugal*; Dias, R., Araújo, A.A., Terrinha, P., Kullberg, J.C., Eds.; Escolar Editora: Lisbon, Portugal, 2013; Volume II-Geologia Meso-Cenozóica de Portugal, pp. 195–348.
32. Carvalho, J.M.F.; Lisboa, J.V.V. Ornamental stone potential areas for land use planning: A case study in a limestone massif from Portugal. *Environ. Earth Sci.* **2018**, *77*, 206; https://doi.org/10.1007/s12665-018-7382-x.
33. Manuppella, G.; Barbosa, B.; Machado, S.; Carvalho, J. *Folha 27-A Vila Nova de Ourém, Carta Geológica de Portugal, Scale 1:50,000*, 2nd ed.; Instituto Geológico e Mineiro: Lisbon, Portugal, 1998.
34. Manuppella, G.; Barbosa, B.; Azerêdo, A.C.; Carvalho, J.; Crispim, J.; Machado, S.; Sampaio, J. *Folha 27-C Torres Novas, Carta Geológica de Portugal, Scale 1:50,000*, 2nd ed.; Instituto Geológico e Mineiro: Lisbon, Portugal, 1999.
35. Azerêdo, A.C. Formalização da litoestratigrafia do Jurássico Inferior e Médio do Maciço Calcário Estremenho (Bacia Lusitânica). *Comun. Geol.* **2007**, *94*, 29–51.
36. Carvalho, J.; Manuppella, G.; Moura, A.C. Portuguese Ornamental Limestones. In Proceedings of International Symposium on Industrial Minerals and Building Stones, Istanbul, Turkey,15–18 September 2003.

37. Cai, Y.; Hu, X.; Li, X.; Pan, Y. Origin of the red colour in a red limestone from the Vispi Quarry section (central Italy): A high-resolution transmission electron microscopy analysis. *Cretac. Res.* **2012**, *38*, 97–102. https://doi.org/10.1016/j.cretres.2011.11.016.
38. Figueiredo, M.O.; Silva, T.P.; Veiga, J.P. Natural Nanomaterials: Reappraising the Elusive Structure of the Nano-sized Mineral Ferrihydrite through X-ray Absorption Spectroscopy at the Iron K-Edge. *Mat. Sci. Forum* **2013**, *730*, 931–935.
39. Figueiredo, M.O.; Silva, T.P.; Veiga, J.P. The blue of iron in mineral pigments: A Fe *K*-edge XANES study of vivianite. *Appl. Phys. A* **2010**, *99*, 357–361. https://doi.org/10.1007/s00339-010-5637-9.
40. No, S.-G.; Park, M.-E.; Yoo, B.-C.; Lee, S.-H. Genesis of Carbonate Breccia Containing Invisible Gold in Taebaeksan Basin, South Korea. *Minerals* **2020**, *10*, 1087. https://doi.org/10.3390/min10121087.
41. Batista, A.F. 2018. Solid as Stone. Forbes Portugal. Available online: https://www.forbespt.com/solido-como-pedra/?geo=pt (accessed on 16 April 2022). (In Portuguese)
42. Carvalho, C.; Silva, Z.; Simão, J. Evaluation of Portuguese limestones' susceptibility to salt mist through laboratory testing. *Environ. Earth Sci.* **2018**, *77*, 523. https://doi.org/10.1007/s12665-018-7670-5.
43. International Commission on Illumination. *CIE 15: Technical Report: Colorimetry*, 3rd ed.; Vienna, Austria, 2004.
44. Silva, T.P.; De Oliveira, D.; Veiga, J.P.; Lisboa, V.; Carvalho, J.; Salas-Colera, E. From yellow, brown to blue/greyish limestone: A Fe *K*-edge study through XANES. In *Book of Abstracts of the 7th ENURS—National Meeting of Portuguese Synchrotron Radiation Users*; Faculdade de Ciências e Tecnologia, Universidade Nova de Lisboa: Caparica, Portugal, 2018; p. 44.
45. Solé, V.A.; Papillon, E.; Cotte, M.; Walter, P.; Susini, J. A multiplatform code for the analysis of energy-dispersive X-ray fluorescence spectra. *Spectrochim. Acta* **2007**, *62*, 63–68. https://doi.org/10.1016/j.sab.2006.12.002.
46. Ravel, B.; Newville, M. ATHENA, ARTEMIS, HEPHAESTUS: data analysis for X-ray absorption spectroscopy using IFEFFIT. *J. Synchrotron Radiat.* **2005**, 12, 537–541. https://doi.org/10.1107/S0909049505012719.
47. Wilke, M.; Farges, F.; Petit, P.-E.; Brown, G.E., Jr.; Martin, F. Oxidation state and coordination of Fe in minerals: An Fe *K*-XANES spectroscopic study. *Amer. Min.* **2001**, *86*, 714–730. https://doi.org/10.2138/am-2001-5-612.
48. Fityk 0.8.2 Program, 2007. Available online: http://www.unipress.waw.pl/fityk (accessed on 16 April 2022).
49. Petit, P.-E.; Farges, F.; Wilke, M.; Solé, V.A. Determination of the iron oxidation state in earth materials using XANES pre-edge information. *J. Synchrotron Radiat*. **2001**, *8*, 952–954. https://doi.org/10.1107/s0909049500021063.
50. Carvalho, C.; Silva, Z.; Simão, J. Surface alteration on limestones exposed to salt mist. *Comum. Geol.* **2018**, *105*, 91–99. (In Portuguese)
51. ICOMOS-ISCS. *Illustrated Glossary on Stone Deterioration Patterns, English-Portuguese Version;* ICOMOS: Paris, France, 2008; p. 80.
52. Zheng, L.Z.; Liang, X.T.; Li, S.R.; Li, Y.H.; Hu, D.D. Fading and showing mechanisms of ancient color relics based on light scattering induced by particles. *RSC Adv.* **2018**, *8*, 1124–1131. https://doi.org/10.1039/c7ra11923b.
53. Verdingovas, V.; Jellesen, M.S.; Ambat, R. Colorimetric visualization of tin corrosion: A method for early stage corrosion detection on printed circuit boards. *Microelectron. Reliab.* **2017**, *73*, 158–166. https://doi.org/10.1016/j.microrel.2017.05.005.
54. Coutinho, M.L.; Veiga, J.P.; Ruivo, A.; Silva, T.P.; Salas-Colera, E.; Bottura-Scardina, S.; Lima, A.; Figueiredo, E.; Cotte, M.; Lima, M.M.R. An insight into the firing conditions of Chinese blue-and-white porcelain through XANES. *J. Anal. At. Spectrom.* **2022**, *37*, 632–640. https://doi.org/10.1039/d2ja00006g.
55. Ruiz-Ardanaz, I.; Lasheras, E.; Durán, A. Mineralogical Characterization of Carreaux de Pavement from Northern Spain (Tiebas, Navarre). *Minerals* **2021**, *11*, 153; https://doi.org/10.3390/min11020153.
56. Barbero-Álvarez, M.A.; Menéndez, J.M.; Rodrigo, J.A.; Ramírez-Barat, B.; Cano, E. Assessment of the Robustness of a Color Monitoring Chart Calibration Method for Crowdsourcing-Based Preventive Conservation. *Appl. Sci.* **2021**, *11*, 10067; https://doi.org/10.3390/app112110067.
57. Instituto Português do Mar e da Atmosfera (IPMA). 2022. Available online: https://www.ipma.pt/pt/publicacoes/boletins.jsp?cmbDep=cli&cmbTema=pcl&idDep=cli&idTema=pcl&curAno=-1 (accessed on 28 May 2022).
58. Pavingexpert, The Curse of Black Limestone. Available online: https://www.pavingexpert.com/stonpv05 (accessed on 16 April 2022).
59. Galvez-Martinez, S.; Mateo-Marti, E. Ultraviolet Irradiation on a Pyrite Surface Improves Triglycine Adsorption. *Life* **2018**, *8*, 50. https://doi.org/10.3390/life8040050.
60. Mateo-Marti, E.; Galvez-Martinez, S.; Gil-Lozano, C.; Zorzano, M.-P. Pyrite-induced uv-photocatalytic abiotic nitrogen fixation: Implications for early atmospheres and Life. *Sci. Rep.* **2019**, *9*, 15311. https://doi.org/10.1038/s41598-019-51784-8.
61. Földvári, M. *Handbook of Thermogravimetric System of Minerals and Its Use in Geological Practice*; Kiadó, F., Ed.; Geological Institute of Hungary: Budapest, Hungary, 2011.
62. Chattaraj, B.D.; Dutta, S.N.; Iyengar, M.S. Studies on the thermal decomposition of calcium carbonate in the presence of alkali salts (Na_2CO_3, K_2CO_3 and NaCl). *J. Therm. Anal.* **1973**, *5*, 43–49. https://doi.org/10.1007/BF01914472.
63. Galoisy, L.; Calas, G.; Arrio, M.A. High-resolution XANES spectra of iron in minerals and glasses: Structural information from the pre-edge region. *Chem. Geol.* **2001**, *174*, 307–319. https://doi.org/10.1016/S0009-2541(00)00322-3.
64. Jheeta, K.S.; Jain, D.C. Investigation of coordination geometry around iron in annealed sapphire (Al_2O_3) using PL, XRD, XAS and FTIR techniques. *Afr. Phys. Rev.* **2007**, *1*, 56–66.
65. Wilke, M.; Partzsch, G.M.; Bernhardt, R.; Lattard, D. Erratum to "Determination of the iron oxidation state in basaltic glasses using XANES at the K-edge". *Chem. Geol.* **2005**, *220*, 143–161. doi:10.1016/j.chemgeo.2004.08.034.

66. Westre, T.E.; Kennepohl, P.; DeWitt, J.G.; Hedman, B.; Hodgson, K.O.; Solomon, E.I. A Multiplet Analysis of Fe K-Edge 1s → 3d Pre-Edge Features of Iron Complexes. *J. Am. Chem. Soc.* **1997**, *119*, 6297–6314. https://doi.org/10.1021/ja964352a.
67. Dräger, G.; Frahm, R.; Materlik, G.; Brümmer, O. On the Multipole Character of the X-Ray Transitions in the Pre-Edge Structure of Fe K Absorption Spectra. An Experimental Study. *Phys. Stat. Sol. B* **1988**, *146*, 287–294; https://doi.org/10.1002/pssb.2221460130.
68. England, K.E.R.; Charnock, J.M.; Pattrick, R.A.D.; Vaughan, D.J. Surface oxidation studies of chalcopyrite and pyrite by glancing-angle X-ray absorption spectroscopy (REFLEXAFS). *Min. Mag.* **1999**, *63*, 559–566. https://doi.org/10.1180/002646199548718.
69. Wasserman, I.; Bentur, A. The efficiency of surface treatments on enhancement of the durability of limestone cladding stones. *Mat. Struct.* **2005**, *38*, 99–105. https://doi.org/10.1617/14068.
70. Todd, E.C.; Sherman, D.M.; Purton, J.A. Surface oxidation of pyrite under ambient atmospheric and aqueous (pH = 2 to 10) conditions: Electronic structure and mineralogy from X-ray absorption spectroscopy. *Geochim. Cosmochim. Acta* **2003**, *67*, 881–893. https://doi.org/10.1016/S0016-7037(02)00957-2.
71. Bladh, K.W. The Formation of Goethite, Jarosite, and Alunite during the Weathering of Sulfide-Bearing Felsic Rock. *Econ. Geol.* **1982**, *77*, 176–184. https://doi.org/10.2113/gsecongeo.77.1.176.
72. Bianco, L. Geochemistry, Mineralogy and Textural Properties of the Lower Globigerina Limestone Used in the Built Heritage. *Minerals* **2021**, *11*, 740. https://doi.org/10.3390/min11070740.\